Mineralogical Magazine (2019), **83**, 81–88
doi:10.1180/minmag.2017.081.095

CAMBRIDGE UNIVERSITY PRESS

New minerals with modular structure derived from hatrurite from the pyrometamorphic rocks. Part IV: Dargaite, $BaCa_{12}(SiO_4)_4(SO_4)_2O_3$, from Nahal Darga, Palestinian Autonomy

Irina O. Galuskina[1], Frank Gfeller[2], Evgeny V. Galuskin[1], Thomas Armbruster[2], Yevgeny Vapnik[3], Mateusz Dulski[4], Mariusz Gardocki[1], Lidia Jeżak[5] and Mikhail Murashko[6]

[1]Faculty of Earth Sciences, Department of Geochemistry, Mineralogy and Petrography, University of Silesia, Będzińska 60, 41-200 Sosnowiec, Poland; [2]Mineralogical Crystallography, Institute of Geological Sciences, University of Bern, Freiestr. 3, CH-3012 Bern, Switzerland; [3]Department of Geological and Environmental Sciences, Ben-Gurion University of the Negev, P.O.B. 653, Beer-Sheva 84105, Israel; [4]Silesian Center for Education and Interdisciplinary Research and Institute of Material Science, 75 Pułku Piechoty 1a, 41-500 Chorzow, Poland; [5]Institute of Geochemistry, Mineralogy and Petrology, Warsaw University, al. Żwirki i Wigury 93, 02-089 Warszawa, Poland; and [6]Saint Petersburg State University, Institute of Earth Sciences, 7-9, Universitetskaya nab., St. Petersburg, 199034, Russia

Abstract

Dargaite, ideally $BaCa_{12}(SiO_4)_4(SO_4)_2O_3$, is an additional member of the arctite group belonging to minerals with a modular intercalated antiperovskite structure derived from hatrurite. The holotype specimen was found at a small outcrop of larnite pseudoconglomerates in the Judean Mts, West Bank, Palestinian Autonomy. Larnite, fluorellestadite–fluorapatite, brownmillerite, fluormayenite–fluorkyuygenite and ye'elimite are the main minerals of the holotype specimen; ternesite, shulamitite and periclase are noted rarely. Dargaite, nabimusaite and gazeevite occur in linear zones with higher porosity within larnite rocks. Pores are filled with ettringite and Ca-hydrosilicates, less commonly with gibbsite, brucite, baryte, katoite and calciolangbeinite. Dargaite is colourless, transparent with a white streak and has a vitreous lustre. It exhibits pronounced parting and imperfect cleavage along (001). Mohs' hardness is ~4.5–5.5. The empirical formula is $(Ba_{0.72}K_{0.24}Na_{0.04})_{\Sigma1}(Ca_{11.95}Mg_{0.04}Na_{0.01})_{\Sigma12}([SiO_4]_{0.91}\ [PO_4]_{0.05}[AlO_4]_{0.03}[Ti^{4+}O_4]_{0.01})_{\Sigma4}([SO_4]_{0.84}[PO_4]_{0.14}[CO_3]_{0.02})_{\Sigma2}(O_{2.54}F_{0.46})_{\Sigma3}$. Dargaite is trigonal $R\bar{3}m$, the unit-cell parameters are: $a = 7.1874(4)$ Å, $c = 41.292(3)$ Å, $V = 1847.32(19)$ Å^3 and $Z = 3$. The crystal structure of dargaite was refined from X-ray single-crystal data to $R_1 = 3.79\%$. The calculated density is 3.235 g cm^{-3}. The following main Raman bands are distinguished on the holotype dargaite (cm^{-1}): 122, 263, 323, 464, 523, 563, 641 and 644, 829 and 869, 947, 991 and 1116. The formation conditions of dargaite are linked to the local occurrence of pyrometamorphic by-products (gases, fluids and melts) transforming earlier mineral associations at ~900°C.

Keywords: dargaite, arctite group, antiperovskite structure, Raman spectrum, pyrometamorphic rocks, Hatrurim Complex

(Received 5 September 2017; accepted 22 November 2017)

Introduction

In pyrometamorphic rocks of the Hatrurim Complex, which have a wide distribution along the Dead Sea Rift in the territories of Israel, Palestinian Autonomy and Jordan ('Mottled zone'; Bentor, 1960; Gross, 1977; Vapnik *et al.*, 2007), seven new minerals with modular intercalated antiperovskite structures derived from hatrurite have been discovered during the last few years (Table 1).

Dargaite with the end-member crystal chemical formula $BaCa_{12}(SiO_4)_4(SO_4)_2O_3$ was found at the same time as isostructural nabimusaite, $KCa_{12}(SiO_4)_4(SO_4)_2O_2F$, in larnite rocks from the Jabel Harmun locality, Palestinian Autonomy. However, a description of dargaite as a new mineral was hampered initially by the grain size (Galuskin *et al.*, 2015*a*). Discovery of larnite pebbles containing relatively large dargaite grains within larnite pseudoconglomerates at the Hahal Darga locality, Palestinian Autonomy, finally permitted a meaningful investigation of this mineral, the results of which we present in this paper.

Dargaite forms a solid solution with nabimusaite, $KCa_{12}(SiO_4)_4(SO_4)_2O_2F$ and ariegilatite, $BaCa_{12}(SiO_4)_4(PO_4)_2OF_2$. It is isostructural to the phosphate mineral arctite, $BaCa_7Na_5(PO_4)_6F_3$ (Table 1; Sokolova *et al.*, 1984). Arctite-group minerals are classified as having intercalated antiperovskite structures (Krivovichev, 2008; Galuskin *et al.*, 2015*a*, *b*), for which octahedra are anion-centred and tetrahedra are cation-centred.

Several phases belonging to the structural type of intercalated antiperovskites have already been described (Table 1). These minerals of the series with end-members zadovite, $BaCa_6[(SiO_4)(PO_4)](PO_4)_2F$ and aradite, $BaCa_6[(SiO_4)(VO_4)](VO_4)_2F$, occur in paralavas of the Hatrurim Complex in the Negev Desert, Israel (Galuskin *et al.*, 2015*b*). Gazeevite, $BaCa_6(SiO_4)_2(SO_4)_2O$, was found in an altered xenolith of the Shadil-Khokh volcano, Sothern Ossetia and at a few localities of larnite pseudoconglomerates of the Hatrurim Complex (Galuskin *et al.*, 2017). Stracherite

Author for correspondence: Irina O. Galuskina, Email: irina.galuskina@us.edu.pl
Associate Editor: Stuart Mills
Cite this article: Galuskina I.O., Gfeller F., Galuskin E.V., Armbruster T., Vapnik Y., Dulski M., Gardocki M., Jeżak L. and Murashko M. (2019) New minerals with modular structure derived from hatrurite from the pyrometamorphic rocks. Part IV: Dargaite, $BaCa_{12}(SiO_4)_4(SO_4)_2O_3$, from Nahal Darga, Palestinian Autonomy. *Mineralogical Magazine*, **83**, 81–88. https://doi.org/10.1180/minmag.2017.081.095

Table 1. A comparison of minerals with modular antiperovskite structure derived from hatrurite discovered in rock of the Hatrurim Complex*, related mineral species and synthetic materials.

Mineral name	Ideal formula	Space group	*a* (Å)	*c* (Å)	*V* (Å^3)	*Z*	Reference
Arctite group							
Arctite	$BaCa_7Na_5(PO_4)_6F_3$	$R\bar{3}m$	7.094	41.320	1800.83	3	Sokolova *et al.* (1984)
Nabimusaite	$KCa_{12}(SiO_4)_4(SO_4)_2O_2F$	$R\bar{3}m$	7.1905(4)	41.251(3)	1847.1(2)	3	Galuskin *et al.* (2015*a*)
Dargaite	$BaCa_{12}(SiO_4)_4(SO_4)_2O_3$	$R\bar{3}m$	7.1874(4)	41.292(3)	1847.32(19)	3	Gfeller *et al.* (2016)
Ariegilatite	$BaCa_{12}(SiO_4)_4(PO_4)_2OF_2$	$R\bar{3}m$	7.1551(6)	41.303(3)	1831.2(3)	3	Galuskin *et al.* (2018*b*)
Zadovite group							
Zadovite	$BaCa_6[(SiO_4)(PO_4)](PO_4)_2F$	$R\bar{3}m$	7.09660(10)	25.7284(3)	1122.13(3)	3	Galuskin *et al.* (2015*b*)
Aradite	$BaCa_6[(SiO_4)(VO_4)](VO_4)_2F$	$R\bar{3}m$	7.1300(1)	26.2033(9)	1153.63(6)	3	Galuskin *et al.* (2015*b*)
Gazeevite	$BaCa_6(SiO_4)_2(SO_4)_2O$	$R\bar{3}m$	7.1540(1)	25.1242(5)	1113.58(3)	3	Galuskin at al. (2017)
Stracherite	$BaCa_6(SiO_4)_2[(PO_4)(CO_3)]F$	$R\bar{3}m$	7.0877(5)	25.201(2)	1096.4(1)	3	Galuskin *et al.* (2018*a*)
Hatrurite	$Ca_3(SiO_4)O$	$R\bar{3}m$	7.135(6)	25.586(15)	1128.031	9	Nishi and Takéuchi (1984)
A synthetic phase	$KCa_{12}(SiO_4)_4(SO_4)_2O_2F$	$R\bar{3}m$	7.197(5)	41.224(28)	1894.20	3	Fayos *et al.* (1985)
A synthetic phase	$Ca_{5.45}Li_{3.55}[SiO_4]_3O_{0.45}F_{1.55}$	$R\bar{3}m$	7.137	41.459	1828.86	6	Krüger (2010)

*Minerals found in the Hatrurim Complex are given in bold font.

Table 2. Representative compositions of dargaite from Nahal Darga (1), Ma'ale Adumim (2) and Shadil-Khokh (3); and ariegilatite from Ma'ale Adumim (4).

	Dargite (1)			Dargite (2)			Dargite (3)	Ariegilatite (4)
n	22			16			3	2
	wt.%	S.D.	Range	wt.%	S.D.	Range	wt.%	wt.%
SO_3	11.25	0.66	9.15–11.48	11.12	0.57	9.23–11.78	12.21	5.35
V_2O_5								0.15
P_2O_5	2.90	0.22	2.70–3.36	2.56	0.57	1.71–4.33	0.30	8.73
TiO_2	0.18	0.03	0.13–0.25	0.13	0.04	0.08–0.19	0.47	0.15
SiO_2	18.26	0.26	17.74–18.76	18.74	0.31	18.28–19.39	19.30	17.15
Fe_2O_3				0.20	0.08	0–0.36	0.30	
Al_2O_3	0.45	0.06	0.34–0.56	0.90	0.14	0.73–1.20	0.32	0.66
BaO	9.21	0.57	8.35–9.93	8.19	0.56	7.49–9.78	10.12	11.40
SrO							0.20	0.14
CaO	55.73	0.54	55.17–56.73	57.19	0.38	56.44–58.02	56.30	55.70
MgO	0.14	0.03	0.10–0.18	0.09	0.01	0.06–0.11	0.06	0.11
K_2O	0.94	0.06	0.85–1.04	1.11	0.17	0.54–1.35	0.73	0.14
Na_2O	0.12	0.02	0.08–0.15	0.25	0.03	0.18–0.28	0.04	0.15
F	0.72	0.05	0.64–0.86	1.32	0.24	0.97–1.53	0.66	1.30
CO_2	0.12			0.11			0.41	0.29
–O = F	0.30			0.45			0.28	0.55
Total	99.71			101.34			101.14	100.87
Atoms per formula unit								
Ba	0.722			0.627			0.787	0.895
Sr							0.023	0.016
K	0.240			0.277			0.185	0.036
Na	0.038			0.095			0.005	0.053
Ca				0.001				
Σ*A*	1.000			1.000			1.000	1.000
Ca	11.950			11.973			11.972	11.961
Na	0.009						0.010	0.006
Mg	0.042			0.027			0.018	0.033
Σ*B*	12.001			12.000			12.000	12.000
Si	3.654			3.662			3.810	3.437
P	0.213			0.082				0.384
Ti^{4+}	0.027			0.019			0.070	0.023
Fe^{3+}				0.030			0.045	
Al	0.106			0.207			0.075	0.156
S^{6+}								
Σ*T*1	4.000			4.000			4.000	4.000
S^{6+}	1.690			1.631			1.819	0.805
P	0.278			0.342			0.050	1.097
Si							0.020	
V^{5+}								0.020
C	0.031			0.028			0.111	0.079
Σ*T*2	1.999			2.001			2.000	2.000
F	0.458			0.813			0.411	0.826
O	0.542			0.187			0.589	0.174
Σ*W*1	1.000			1.000			1.000	1.000
F								
O	2.000			2.000			2.000	2.000
Σ*W*2	2.000			2.000			2.000	2.000

n = number of analyses; S.D. = standard deviation.

$BaCa_6(SiO_4)_2[(PO_4)(CO_3)]F$ (Galuskin *et al.*, 2018*a*), was discovered recently in spurrite rocks of the Hatrurim Complex in the Negev Desert.

The structure type of the arctite group (3:1 type) is described by the formula $AB_{12}(TO_4)_4(TO_4)_2W_3$, while the zadovite group (1:1 type) has the formula $AB_6(TO_4)_2(TO_4)_2W$; where A = Ba, K, Sr…; B = Ca, Na…; T = Si, P, V^{5+}, S^{6+}, Al…; and $W = O^{2-}$, F^- (Table 1). Antiperovskite single $\{[WB_6](TO_4)_2\}$ layers in the zadovite-type structure and triple $\{[W_3B_{12}](TO_4)_4\}$ layers in the arctite type intercalate with single $A(TO_4)_2$ layers (Gfeller *et al.*, 2013; Galuskin *et al.*, 2015*a*,*b*; Galuskin *et al.*, 2017, 2018*a*,*b*). In stracherite, $BaCa_6(SiO_4)_2[(PO_4)(CO_3)]F$, half of the tetrahedral sites in the $A(TO_4)_2$ layer are partly substituted by CO_3 triangles (Galuskin *et al.*, 2018*a*).

The mineral is named after the Canyon (Nahal) Darga, near to where it was first discovered, and which is the type locality in the Judean Mts, West Bank, Palestinian Autonomy, Israel. Type material has been deposited in the mineralogical collection of the Fersman Mineralogical Museum, Leninskiy pr., 18/k2, 115162 Moscow, Russia, catalogue number 4713/2 (this specimen also is co-type for gazeevite, author's number DR5D, Nahal Darga).

Methods

Crystal morphology and chemical composition of dargaite and associated minerals were examined using optical microscopes and a Philips XL30 ESEM/EDAX analytical electron scanning microscope (Faculty of Earth Sciences, University of Silesia, Poland). Chemical analyses of dargaite were performed with a CAMECA SX100 microprobe (Institute of Geochemistry, Mineralogy and Petrology, University of Warsaw, Poland) at 15 kV and 20 nA using the following lines and standards: Ba*L*α and S*K*α – baryte; P*K*α – apatite; Ca*K*α – wollastonite; Mg*K*α and Si*K*α – diopside; Fe*K*α – hematite; Al*K*α and K*K*α – orthoclase; Ti*K*α – rutile; Na*K*α – albite; Sr*L*α – $SrTiO_3$; and F*K*α – fluorphlogopite.

The Raman spectrum of dargaite was recorded on a WITec alpha 300R Confocal Raman Microscope (Department of Earth Science, University of Silesia, Poland) equipped with an air-cooled solid laser (532 nm) and a CCD camera operating at –61°C. The laser radiation was coupled to a microscope through a single-mode optical fibre with a diameter of 3.5 μm. An air Zeiss LD EC Epiplan-Neofluan DIC – 100/0.75NA objective was used. Raman-scattered light was focused on a broad band single mode fibre with effective pinhole size ~30 μm and using a monochromator with a 600 mm^{-1} grating. The power of the laser at the sample position was 42 mW. Integration times of 3 s with accumulation of 15 scans and a resolution 3 cm^{-1} were chosen. The monochromator was calibrated using the Raman-scattering line of a silicon plate (520.7 cm^{-1}).

Single-crystal X-ray studies were carried out on a dargaite grain ~0.03 mm × 0.03 mm × 0.02 mm in size, using a Bruker APEX II SMART diffractometer (Mo*K*α, λ = 0.71073 Å; University of Bern, Switzerland). Experimental details are summarised in Table 3. Diffraction data were collected with ω scans at different φ settings (φ-ω scan) (Bruker, 1999). Data were processed using *SAINT* (Bruker, 1999). An empirical absorption correction using *SADABS* (Sheldrick, 1996) was applied. The structure of nabimusaite (Fayos *et al.*, 1985; Galuskin *et al.*, 2015*a*) was taken as the initial model. Subsequently the structure was refined using the program *SHELX97* (Sheldrick, 2008) to R_1 = 3.79%. The refinements including anisotropic atom displacement-parameters were carried out with neutral atom scattering-factors (Tables 3–6). The crystallographic information file has been deposited with the Principal Editor of *Mineralogical Magazine* and is available as Supplementary material (see below).

Table 3. Crystal data, X-ray measurement and refinement parameters for dargaite.

Crystal data	
Formula (from X-ray data)	$Ba_{0.7}K_{0.3}Ca_{12}(SiO_4)_4(SO_4)_2[O_{2.5}F_{0.5}]$
Unit-cell dimensions (Å)	a = 7.1874(4), c = 41.292(3)
Space group	$R\bar{3}m$ (No. 166)
Volume (Å^3)	1847.32(19)
Z	3
Calculated density (g cm^{-3})	3.235
Data collection	
Crystal size (mm)	0.03 × 0.03 × 0.02
Diffractometer	APEX II SMART
X-ray radiation, wavelength (Å)	Mo*K*α, 0.71073
X-ray power	50 kV, 30 mA
Monochromator	Graphite
Temperature (K)	293
Detector-to-sample distance (cm)	5
Measurement method	Phi and Omega scans
Time per frame	30 s
Max. θ° range for data collection	27.94
Index ranges	$-8 \le h \le 9$, $-8 \le k \le 9$, $-53 \le l \le 54$
No. of measured reflections	6106
No. of unique reflections	620
No. of observed reflections [$I > 2\sigma$ (I)]	396
Refinement	
No. of parameters used in refinement	57
R_{int}	0.1105
R_σ	0.0810
R_1, $I > 2\sigma(I)$	0.0376
R_1 all Data	0.0679
$wR2$ on (F^2)	0.0727
GoF	0.865
Δρ max (e^- Å^{-3})	0.78 close to O4
Δρ min ($-e^-$ Å^{-3})	−0.82 close to O4

Occurrence and description of dargaite

The holotype specimen (larnite pebble 3.5 cm in size) containing relatively large dargaite aggregates (up to 100–150 μm in size) of dargaite grains (up to 30–40 μm in size) (Fig. 1*a*, *b*) was found at one small outcrop of larnite pseudoconglomerates in the Judean Mts, West Bank, Palestinian Autonomy (31°36.5'N, 35°22.7'E).

Table 4. Atom coordinates, occupancies and U_{eq} (Å^2) values for dargaite.

Site	Atom	x	y	z	U_{eq}	Occ.
Ba1	Ba	0	0	0	0.0264(5)	0.702(6)
	K	0	0	0	0.0264(5)	0.297(6)
Ca1	Ca	0.15793(10)	0.84207(10)	0.39826(3)	0.0172(3)	1
Ca2	Ca	0.15188(10)	0.84812(10)	0.53235(3)	0.0166(4)	1
S	S	0	0	0.67548(6)	0.0148(6)	1
Si1	Si	0	0	0.20631(7)	0.0131(7)	1
Si2	Si	0	0	0.08193(7)	0.0122(7)	1
O1	O	0.5547(3)	0.4453(3)	0.64542(9)	0.0218(11)	1
O2	O	0.1247(3)	0.8753(3)	0.19437(10)	0.0230(11)	1
O3	O	0.1237(3)	0.8763(3)	0.07045(10)	0.0213(11)	1
O4	O	0	0	0.36040(16)	0.0171(17)	1
O5	O	0	0	0.75353(16)	0.0204(18)	1
O6	O	0	0	0.12140(16)	0.0171(17)	1
O7	O	0	0	0.43010(14)	0.0125(15)	0.77
	F	0	0	0.43010(14)	0.0125(15)	0.23*
O8	O	0	0	½	0.007(2)	1

*F at O7 fixed according to results of chemical analyses; Occ. = occupancy

Table 5. Anisotropic displacement parameters U^{ij} (Å^2) for dargaite.

Site	U^{11}	U^{22}	U^{33}	U^{23}	U^{13}	U^{12}
Ba1	0.0244(6)	0.0244(6)	0.0303(8)	0	0	0.0122(3)
Ca1	0.0137(5)	0.0137(5)	0.0244(7)	−0.0005(3)	0.0005(3)	0.0070(6)
Ca2	0.0135(5)	0.0135(5)	0.0221(7)	0.0009(3)	−0.0009(3)	0.0061(6)
S	0.0146(9)	0.0146(9)	0.0151(13)	0	0	0.0073(5)
Si1	0.0093(10)	0.0093(10)	0.0207(17)	0	0	0.0046(5)
Si2	0.0088(10)	0.0088(10)	0.0191(16)	0	0	0.0044(5)
O1	0.026(2)	0.026(2)	0.022(2)	0.0007(10)	−0.0007(10)	0.020(2)
O2	0.0158(19)	0.0158(19)	0.039(3)	−0.0019(10)	0.0019(10)	0.009(2)
O3	0.0161(19)	0.0161(19)	0.032(3)	−0.0028(10)	0.0028(10)	0.009(2)
O4	0.019(3)	0.019(3)	0.013(4)	0	0	0.0097(13)
O5	0.022(3)	0.022(3)	0.017(4)	0	0	0.0111(14)
O6	0.017(3)	0.017(3)	0.018(4)	0	0	0.0084(13)
O7	0.011(2)	0.011(2)	0.016(4)	0	0	0.0054(11)
O8	0.005(3)	0.005(3)	0.010(5)	0	0	0.0026(16)

This outcrop including neighbouring hills of pyrometamorphic rocks, is known under the common name 'Nahal Darga' (see geological scheme in Novikov *et al.*, 2013). These outcrops are located ~1–1.5 km to the north of the well-known tourist site: Canyon (Nahal) Darga, located close to the west shore of the Dead Sea.

Larnite, fluorellestadite–fluorapatite, brownmillerite, fluormayenite–fluorkyuygenite and ye'elimite are the main minerals of the holotype specimen; ternesite, shulamitite and periclase are rarely present. Dargaite, nabimusaite and gazeevite occur in linear zones of higher porosity embedded in massive larnite rocks (Fig. 1*a*). Pores are filled with ettringite and Ca-hydrosilicates, less commonly with gibbsite, brucite, baryte, katoite and calciolangbeinite. It is notable that fluorkyuygenite has a considerable distribution in these linear zones. In the groundmass fluormayenite with ye'elimite rims prevails (Środek *et al.*, 2018).

Dargaite is colourless, transparent with white streak and vitreous lustre, it shows no ultraviolet luminescence. Dargaite is brittle and exhibits pronounced parting and imperfect cleavage along (001). Dargaite is uniaxial (–), $\omega = 1.643(3)$, $\varepsilon = 1.639(3)$ (589 nm) and has no pleochroism. Mohs hardness is ~4.5–5.5 and mean VHN = 423 kg/mm^2 (load 50 g, range 380–492 kg/mm^2, 14 measurements). Density could not be measured because of abundant tiny inclusions of ye'elimite and larnite; the calculated density is 3.235 g cm^{-3}. The Gladstone–Dale compatibility factor is $[1 - (K_p/K_c)] = -0.007$, superior (Mandarino, 1981) using the empirical formula.

Table 6. Selected interatomic distances (Å) for dargaite.

Ba1–O1 ×6	2.892(4)	S–O1 ×3	1.486(4)
Ba1–O3 ×6	3.291(4)	S–O4	1.482(7)
<Ba–O>	3.092	<S–O>	1.485
Ca1–O1 ×2	2.631(3)	Si1–O2 ×3	1.629(4)
Ca1–O2	3.121(4)	Si1–O5	1.658(7)
Ca1–O3 ×2	2.366(3)	<Si1–O>	1.637
Ca1–O4	2.512(4)		
Ca1–O5	2.364(3)	Si2–O3 ×3	1.611(4)
Ca1–O7	2.365(4)	Si2–O6	1.630(7)
<Ca1–O>	2.544	<Si2–O>	1.616
Ca2–O2 ×2	2.333(3)	O7–Ca1 ×3	2.356(4)
Ca2–O2	2.578(4)	O7–Ca2 ×3	2.445(4)
Ca2–O3	2.733(4)	<O7–O>	2.401
Ca2–O6	2.321(2)		
Ca2–O7	2.445(4)	O8–Ca2 ×6	2.315(1)
Ca2–O8/F8	2.315(1)		
<Ca2–O>	2.437		

The empirical formula is $(Ba_{0.72}K_{0.24}Na_{0.04})_{\Sigma1}(Ca_{11.95}Mg_{0.04}Na_{0.01})_{\Sigma12}([SiO_4]_{0.91}[PO_4]_{0.05}[AlO_4]_{0.03}[Ti^{4+}O_4]_{0.01})_{\Sigma4}([SO_4]_{0.84}[PO_4]_{0.14}[CO_3]_{0.02})_{\Sigma2}(O_{2.54}F_{0.46})_{\Sigma3}$ (Table 2). Considering the prevailing occupants at structural sites, the end-member formula is $BaCa_{12}(SiO_4)_4(SO_4)_2O_3$.

The compositional variation of dargaite found in larnite rocks of the Hatrurim Complex at Ma'ale Adumim locality, Palestinian Autonomy and in altered carbonate xenolith from the lava bed of the Shadi-Khokh volcano, Southern Ossetia (Fig. 1*c*,*d*) is shown in Table 2. Higher P contents are characteristic of dargaite from larnite rocks of the Hatrurim Complex compared to dargaite from Southern Ossetia (Table 2, Galuskin *et al.*, 2015*a*).

Empirical formulae calculated from microprobe analyses on the basis of 19 cations for dargaite from different localities show an overestimation of cations (>13 atoms per formula unit) at the Ba and Ca sites. These overly high numbers may be due to neglecting the light 'tetrahedral' cations in the analytical procedure. Occurrence of stracherite, $BaCa_6(SiO_4)_2[(PO_4)(CO_3)]F$ (Galuskin *et al.*, 2018*a*) and ariegilatite, $BaCa_{12}(SiO_4)_4(PO_4)_2F_2O$, in spurrite rocks of the Hatrurim Complex, with CO_3 contents above 1 wt.% (Galuskin *et al.*, 2018*a*), strongly suggests that C is most probably the missing cation in dargaite. The presence of CO_3^{2-} groups in dargaite from different localities is confirmed by weak Raman bands at ~1080 cm^{-1} (see below). Calculated data show that CO_3 contents in dargaite are very low (<0.1 atoms per formula unit, Table 2) and do not influence the general crystal chemical conclusions.

Raman spectroscopy study and structure of dargaite

Raman spectra of the holotype dargaite from Nahal Darga and also for dargaite from Ma'ale Adumim and Shadil-Khokh (Fig. 2) were obtained. The spectra correspond to those of Ba-bearing nabimusaite (Galuskin *et al.*, 2015*b*); the following main bands are distinguished on spectra of the holotype dargaite (Fig. 2, cm^{-1}): 70, 122, 129, 263 and 323 (lattice mode, Ba–O, Ca–O vibrations); 401 [$\nu_2(SiO_4)^{4-}$]; 464 [$\nu_2(SO_4)^{2-}$]; 523 [$\nu_4(SiO_4)^{4-}$]; 563 [$\nu_4(PO_4)^{3-}$]; 641 and 644 [$\nu_4(SO_4)^{2-}$]; 829 and 869 [$\nu_1(SiO_4)^{4-}$]; 947 [$\nu_1(PO_4)^{3-}$]; 991 [$\nu_1SO_4)^{2-}$]; 1078 [$\nu_1(CO_3)^{2-}$?]; and 1116 [$\nu_3(SO_4)^{2-}$]. Dargaite from Southern Ossetia contains only negligible P content and thus lacks the characteristic Raman band near 950 cm^{-1}. The band at 1080 cm^{-1} related to vibrations of CO_3 groups is easily detectable. Dargaite from Ma'ale Adumim contains up to 4.33 wt.% P_2O_5 (Table 2) and produces a strong Raman band at 947 cm^{-1} [$\nu_1(PO_4)^{3-}$]. Bands at ~2270,

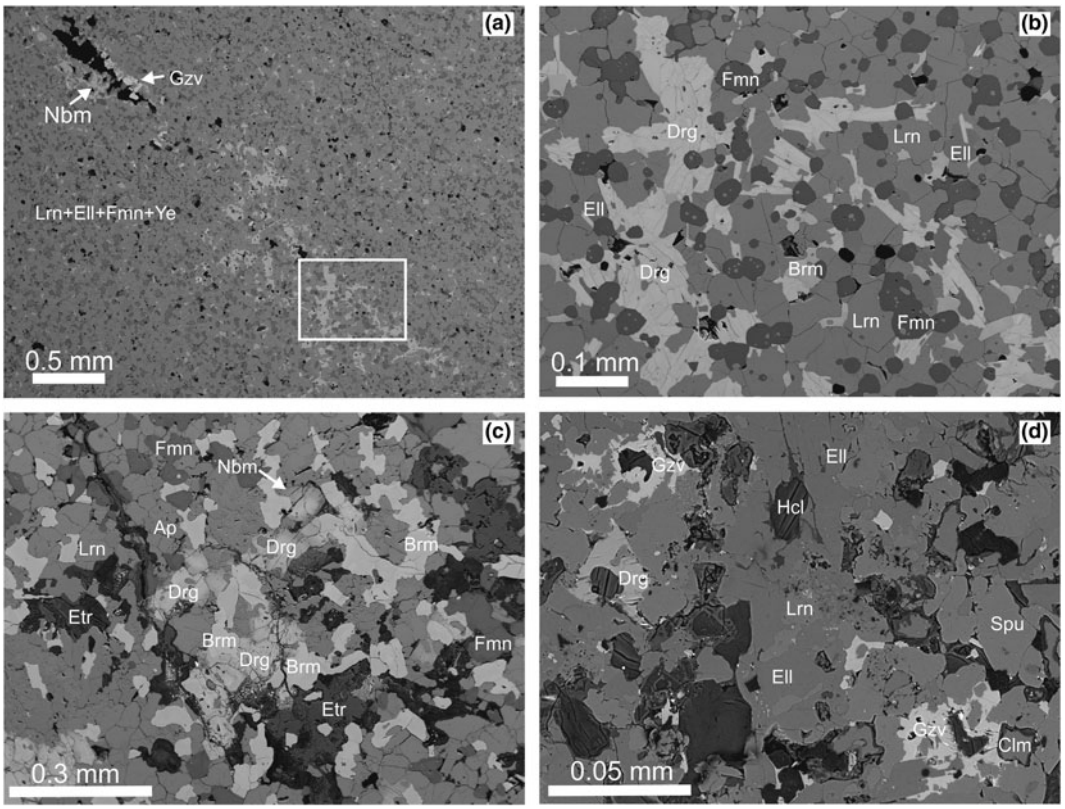

Fig. 1. (*a*) Dargaite is confined to linear porous zones in larnite rock, in which nabimusaite and gazeevite also occur, in the holotype specimen, Nahal Darga. The white frame shows the location magnified in Fig. 1b; (*b*) dargaite aggregates replace fluorellestadite and partially larnite; (*c*) xenomorphic dargaite grains in larnite rock from Ma'ale Adumim; and (*d*) very rare dargaite grains found in altered carbonate xenolith of the Shadil-Khokh volcano at the boundary of larnite (merwinite) and spurrite zones. Drg = dargaite, Ell = fluorellestadite, Lrn = larnite, Fmn = fluormayenite-fluorkyuygenite, Brm = brownmillerite, Ye = ye'elimite, Nbm = nabimusaite, Gzv = gazeevite, Ap = fluorapatite, Etr = ettringite, Hcl = hydrocalumite, Spu = spurrite and Clm = chlormayenite.

2476, 3474 and 3630 cm^{-1} observed on all Raman spectra might be interpreted as: (1) overtones (e.g. ν_3); (2) combinational bands (e.g. $\nu_3+\nu_4$); or (3) artefacts of a layered mineral structure with strong scattered properties of such a system.

A doublet at 830 and 870 cm^{-1} [$\nu_1(SiO_4)^{4-}$] (Fig. 2) relates to the two types of $(SiO_4)^{4-}$ tetrahedra in antiperovskite layers of dargaite (Table 4). This doublet is distinctive in the Raman spectra of dargaite, $BaCa_{12}(SiO_4)_4(SO_4)_2O_3$ and is different to the spectrum of gazeevite, $BaCa_6(SiO_4)_2(SO_4)_2O$. In gazeevite there is only the one type of $(SiO_4)^{4-}$ tetrahedra associated with only one strong band at 865 cm^{-1} (Fig. 2; Galuskin *et al.*, 2017*a*).

Dargaite is isostructural with nabimusaite and its synthetic analogue (Fayos *et al.*, 1985; Galuskin *et al.*, 2015*a*). Dargaite is trigonal with space group $R\bar{3}m$. The unit-cell parameters are: $a = 7.1874(4)$ Å, $c = 41.292(3)$ Å, $V = 1847.32(19)$ $Å^3$ and $Z = 3$. The structure is formed by three-layered antiperovskite modules $\{O_3Ca_{12}(SiO_4)_4\}^{2+}$ interstratified with $Ba(SO_4)_2^{2-}$ layers (Fig. 3). In the nabimusaite structure the antiperovskite module $\{FO_2Ca_{12}(SiO_4)_4\}^{3+}$ intercalates with $K(SO_4)_2^{3-}$ layers (Galuskin *et al.*, 2015*a*). Both antiperovskite modules in dargaite and nabimusaite are derived from hatrurite (Gfeller *et al.*, 2013). The main difference is that the $(SiO_4)^{4-}$ tetrahedra inside the antiperovskite layer of hatrurite have the tetrahedral apices pointing in the same direction whereas in nabimusaite–dargaite the apices alternate pointing up and down (Galuskin *et al.*, 2015*a*). The structural formula of dargaite $Ba_{0.7}K_{0.3}Ca_{12}(SiO_4)_4(SO_4)_2[O_{2.5}F_{0.5}]$ is close to the empirical formula of the holotype specimen (Table 2).

We could not collect meaningful powder diffraction data because of a limited amount of dargaite and difficulties obtaining pure material due to inclusions and admixtures of other minerals. Therefore, a calculated powder diffraction pattern from the structural data is given in Table 7.

Discussion

Dargaite belongs to the arctite structural type (Sokolova *et al.*, 1984; Galuskin *et al.*, 2017). We suggest that the structural formula $AB1_6B2_6[(T1O_4)_2(T2O_4)_2](T3O_4)_2W1_2W2$ of the arctite-group minerals should be simplified to $AB_{12}(TO_4)_4(TO_4)_2W_3$ with combined sites *B1* and *B2*, *T1* and *T2*, and *W1* and *W2*. In this organisation, the formulas of nabimusiate and ariegilatite contain only one double occupied *W* site (made of *W1* = O7 and *W2* = O8) $KCa_{12}(SiO_4)_4(SO_4)_2[O_2F]$ and $BaCa_{12}(SiO_4)_4(PO_4)_2[OF_2]$, respectively. In dargaite, $BaCa_{12}(SiO_4)_4(SO_4)_2[O_3]$, all sites have unique occupation. In arctite, $Ba(Ca_7Na_5)(PO_4)_4(PO_4)_2F_3$, combined occupation is only observed for the *B* site.

Nabimusaite, $KCa_{12}(SiO_4)_4(SO_4)_2O_2F$, daragite $BaCa_{12}(SiO_4)_4(SO_4)_2O_3$ and ariegilatite $BaCa_{12}(SiO_4)_4(PO_4)_2OF_2$ form a continuous solid-solution series (Galuskin *et al.*, 2015*a*, 2017*c*; Table 2). The main isomorphic scheme in the nabimusaite–dargaite series is $^{A}K^{+} + {}^{W}F^{-} \rightarrow {}^{A}Ba^{2+} + {}^{W}O^{2-}$, in the dargaite–ariegilatite

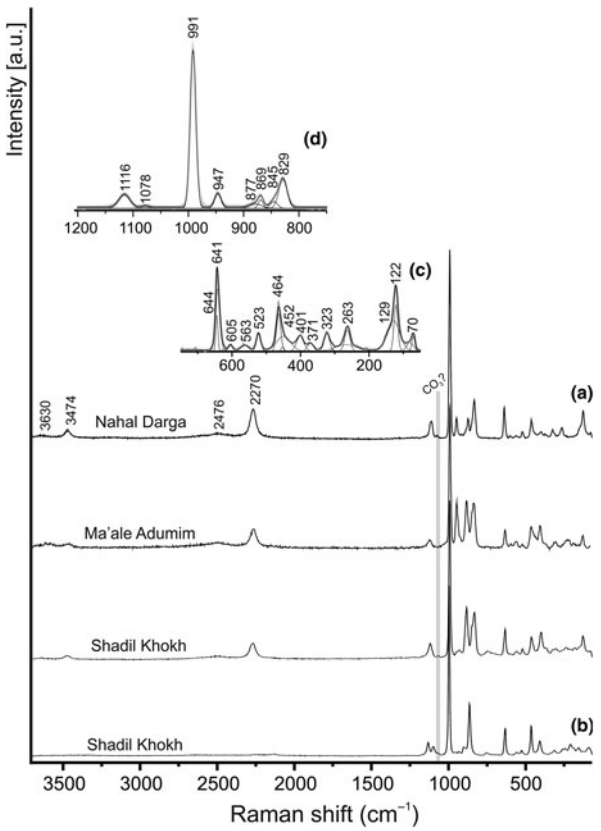

Fig. 2. Raman spectra of dargaite from the three localities (*a*) in comparison with gazeevite spectrum (*b*); and (*c* and *d*) fitting results of holotype dargaite Raman spectrum in the ranges 60–750 and 750–1200 cm^{-1}, respectively.

series: $^{T}(SO_4)^{2-} + {}^{W}O^{2-} \rightarrow {}^{T}(PO_4)^{3-} + {}^{W}F^{-}$, and in the nabimusaite–ariegilatite series: $^{AT}K(SO_4)_2^{3-} + {}^{W}O^{2-} \rightarrow {}^{AT}Ba(PO_4)_2^{4-} + {}^{W}F^{-}$ or expressed in two separate schemes: (1) $^{A}K^{+} + {}^{T}(SO_4)^{2-} \rightarrow {}^{A}Ba^{2+} + {}^{T}(PO_4)^{3-}$; and (2) $^{T}(SO_4)^{2-} + {}^{W}O^{2-} \rightarrow {}^{T}(PO_4)^{3-} + {}^{W}F^{-}$. Isomorphic substitutions in the tetrahedral layer $A(TO_4)_2$ of the nabimusaite–dargaite and dargaite–ariegilatite series are balanced by the O/F ratio variation within the antiperovskite modules $\{[W_3Ca_{12}](SiO_4)_4\}$. In the nabimusaite–ariegilatite series a substitution of $(SO_4)^{2-}$ for $(PO_4)^{3-}$ is balanced by $K^{+} \rightarrow Ba^{2+}$ in the tetrahedral layer and/or O → F in the antiperovskite module.

The authors refining the structure of the synthetic phase, $KCa_{12}(SiO_4)_4(SO_4)_2O_2F$, assigned fluorine to the central antiperovskite layer (Fayos *et al.*, 1985), corresponding to *O*8 in Table 4. In the case of its natural analogue – nabimusaite, the model with fluorine in the central antiperovskite layer was also adopted for structure refinement (Galuskin *et al.*, 2015*a*). However, calculation of bond-valence sums (Brown and Altermatt, 1985) for dargaite, nabimusaite and synthetic $KCa_{12}(SiO_4)_4(SO_4)_2O_2F$ (Supplementary Tables S1–S3) suggested that F enters the external antiperovskite layers (*O*7Ca_6 octahedral layers, Fig. 3). Thus, the original model has to be revised. In arctite, $BaCa_7Na_5(PO_4)_6F_3$, F occupies the central and the external antiperovskite layer (corresponding to *O*7 and *O*8). In contrast to other minerals of the arctite structure type, in arctite fluorine incorporation in the central antiperovskite layer (corresponding to *O*8) is favoured by the substitution Na → Ca at the F coordinated octahedral site (Sokolova *et al.*, 1984).

The holotype dargaite, $(Ba_{0.72}K_{0.24}Na_{0.04})_{\Sigma1}(Ca_{11.95}Mg_{0.04}Na_{0.01})_{\Sigma12}([SiO_4]_{0.91}[PO_4]_{0.05}[AlO_4]_{0.03}[Ti^{4+}O_4]_{0.01})_{\Sigma4}([SO_4]_{0.84}[PO_4]_{0.14}[CO_3]_{0.02})_{\Sigma2}O_{2.54}F_{0.46}$, represents a solid solution between dargaite,

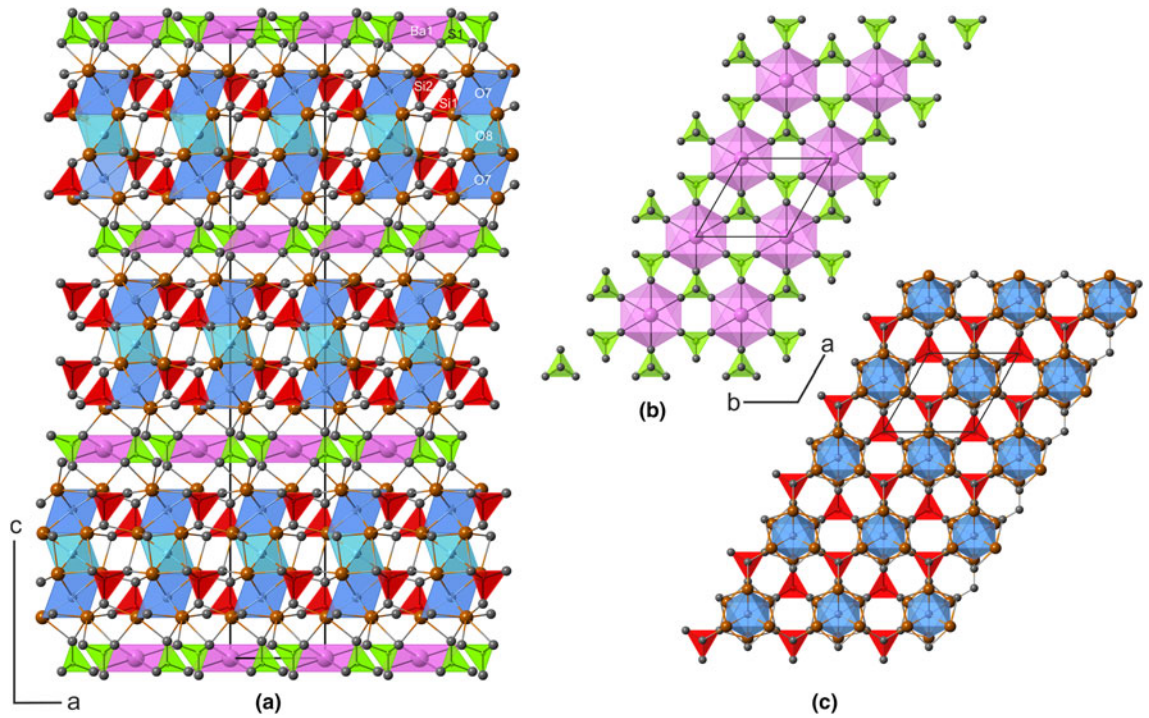

Fig. 3. (*a*) The crystal structure of dargaite along [010]. Ca atoms are shown as brown spheres, SiO_4 tetrahedra in red, SO_4 tetrahedra in green and BaO_6 octahedra in pink. The structure is characterised by modules of three face-sharing antiperovskite type $[OCa_6]$ octahedra (blue). The triplets extend along the threefold axis at (0, 0, *z*), (⅓, ⅓, *z*) and (⅔, ⅔, *z*). Dargaite is isostructural to nabimusaite, $KCa_{12}(SiO_4)_4(SO_4)_2O_2F$. The octahedral F site in nabimusaite is occupied by O (blue) in dargaite, $BaCa_{12}(SiO_4)_4(SO_4)_2O_3$. (*b*,*c*) The antiperovskite modules $\{Ca_{12}(SiO_4)_4O_3\}^{2+}$ in dargaite (*c*), are intercalated by $Ba(SO_4)_2^{2-}$ slices (*b*).

Table 7. Calculated powder diffraction pattern of dargaite*.

I_{calc}	d_{hkl}	h	k	l	I_{calc}	d_{hkl}	h	k	l
8	13.764	0	0	3	14	2.185	1	$\bar{2}$	15
12	6.882	0	0	6	27	2.185	2	$\bar{3}$	$\bar{7}$
15	6.155	1	$\bar{1}$	$\bar{1}$	**43**	**2.141**	**2**	$\bar{2}$	$\bar{14}$
9	4.971	1	0	$\bar{5}$	33	2.141	2	1	$\bar{8}$
13	4.588	0	0	9	9	2.075	3	$\bar{3}$	0
4	4.282	0	1	$\bar{7}$	3	2.052	3	$\bar{3}$	3
16	3.594	2	$\bar{1}$	0	35	1.987	2	0	$\bar{16}$
5	3.441	0	0	$\bar{12}$	32	1.986	3	$\bar{3}$	6
13	3.441	0	1	$\bar{10}$	16	1.890	3	$\bar{3}$	$\bar{9}$
4	3.185	2	$\bar{1}$	$\bar{6}$	**62**	**1.797**	**2**	$\bar{4}$	**0**
100	**3.103**	**2**	$\bar{2}$	**1**	3	1.782	2	$\bar{4}$	3
19	3.077	2	$\bar{2}$	$\bar{2}$	4	1.777	3	$\bar{3}$	$\bar{12}$
5	2.912	0	2	$\bar{5}$	5	1.739	3	$\bar{2}$	$\bar{16}$
11	2.829	0	1	$\bar{13}$	3	1.739	4	$\bar{2}$	$\bar{6}$
21	2.829	2	$\bar{1}$	$\bar{9}$	3	1.725	4	$\bar{3}$	1
95	**2.753**	**0**	**2**	**7**	3	1.721	0	0	$\bar{24}$
88	**2.750**	**0**	**0**	**15**	6	1.720	0	2	$\bar{20}$
8	2.665	1	$\bar{1}$	14	9	1.657	3	$\bar{3}$	$\bar{15}$
63	**2.665**	**0**	**2**	$\bar{8}$	4	1.637	$\bar{3}$	$\bar{3}$	$\bar{8}$
6	2.485	1	$\bar{2}$	12	9	1.607	2	0	$\bar{22}$
3	2.349	2	$\bar{3}$	$\bar{1}$	10	1.555	0	2	$\bar{23}$
3	2.337	2	$\bar{3}$	2	8	1.555	4	$\bar{4}$	$\bar{1}$
9	2.294	0	0	$\bar{18}$	6	1.552	1	$\bar{2}$	24
6	2.223	2	0	$\bar{13}$	**58**	**1.539**	**3**	$\bar{3}$	**18**

*Conditions: Cu$K\alpha_{1+2}$ = 1.540598, Debye-Scherrer geometry, I > 2.00. The strongest lines are given in bold

$BaCa_{12}(SiO_4)_4(SO_4)_2O_3$, nabimusaite, $KCa_{12}(SiO_4)_4(SO_4)_2O_2F$ and ariegilatite, $BaCa_{12}(SiO_4)_4(PO_4)_2OF_2$, with a small contribution of an exotic end-member, for example, $BaCa_{12}[(SiO_4)_2(PO_4)_2](PO_4)_2O_3$ (Table 2). Predominance of Ba at the *A* site (Ba > K + Na) and O at the *W* site (O > F) is the basis for distinguishing the new mineral, the Ba-analogue of nabimusaite. In the dargaite–nabimusaite and dargaite–ariegilatite series, isomorphic substitutions $^{A}Ba^{2+} + {}^{W}O^{2-} \rightarrow {}^{A}K^{+} + {}^{W}F^{-}$ and $^{T}(SO_4)^{2-} + {}^{W}O^{2-} \rightarrow {}^{T}(PO_4)^{3-} + {}^{W}F^{-}$, respectively, have a significant effect on: (1) the increase of F content in dargaite, e.g. K- and P-bearing dargaite from Ma'ale Adumim: $(Ba_{0.63}K_{0.28}Na_{0.09})_{\Sigma1}(Ca_{11.97}Mg_{0.03})_{\Sigma12}([SiO_4]_{0.92}[PO_4]_{0.02}[AlO_4]_{0.05}[FeO_4]_{0.01})_{\Sigma4}([SO_4]_{0.82}[PO_4]_{0.17}[CO_3]_{0.01})_{\Sigma2}O_{2.19}F_{0.81}$(Table 2, an. 2); and (2) the decrease of F content in ariegilatite, e.g. S-bearing ariegilatite from Ma'ale Adumim: $(Ba_{0.90}K_{0.04}Na_{0.05}Sr_{0.01})_{\Sigma1}(Ca_{11.96}Mg_{0.03}Na_{0.01})_{\Sigma12}([SiO_4]_{0.86}[PO_4]_{0.09}[AlO_4]_{0.04}[TiO_4]_{0.01})_{\Sigma4}([PO_4]_{0.55}[SO_4]_{0.40}[CO_3]_{0.04}[VO_4]_{0.01})_{\Sigma2}O_{2.17}F_{0.83}$ (Table 2, an. 4).

Formation conditions of the nabimusaite–dargaite series and associated gazeevite have been discussed before (Galuskin *et al.*, 2015*a*, 2017). Minerals with the intercalated antiperovskite structure derived from hatrurite form at hot spots under the influence of pyrometamorphic by-products (gases, fluids and melts) on minerals of an early clinker association, such as larnite, fluorellestadite and ye'elimite (Galuskin *et al.*, 2016). Paragenesis of ternesite, $Ca_5(SiO_4)_2SO_4$, with minerals of the dargaite–nabimusaite series allows estimation of the temperature of this assemblage at ~900°C (Galuskin *et al.*, 2015*a*).

Acknowledgements. The authors thank Fernando Cámara, Pete Leverett and Ramiza Rastsvetaeva for their careful revisions that improved the early version of the manuscript. The work was supported by the National Science Centre (NCN) of Poland, grant no. 2016/23/B/ST10/00869.

Supplementary material. To view supplementary material for this article, please visit https://doi.org/10.1180/minmag.2017.081.095

References

Bentor Y.K. (editor) (1960) Israel. In: *Lexique Stratigraphique International, Asie*, Vol. III, (10.2). Centre national de la recherche scientifique, Paris.

Brown I.D. and Altermatt D. (1985) Bond-valence parameters obtained from a systematic analysis of the inorganic crystal structure database. *Acta Crystallographica*, **B41**, 244–247.

Bruker (1999) *SMART and SAINT-Plus*. Versions 6.01. Bruker AXS Inc., Madison, Wisconsin, USA.

Fayos J., Glasser F.P., Howie R.A., Lachowski E. and Perez-Mendez M. (1985) Structure of dodecacalcium potassium fluoride dioxide tetrasilicate bis (sulphate), $KF.2[Ca_6(SO_4)(SiO_4)_2O]$: a fluorine-containing phase encountered in cement clinker production process. *Acta Crystallographica*, **C41**, 814–816.

Galuskin E.V., Gfeller F., Armbruster T., Galuskina I.O., Vapnik Ye., Murashko M., Wodyka R. and Dzierżanowski P. (2015*a*) New minerals with modular structure derived from hatrurite from the pyrometamorphic Hatrurim Complex, Part I: Nabimusaite, $KCa_{12}(SiO_4)_4(SO_4)_2O_2F$, from larnite rock of the Jabel Harmun, Palestinian Autonomy, Israel. *Mineralogical Magazine*, **79**, 1061–1072.

Galuskin E.V., Gfeller F., Galuskina I.O., Pakhomova A., Armbruster T., Vapnik Y., Włodyka R., Dzierżanowski P. and Murashko M. (2015*b*) New minerals with modular structure derived from hatrurite from the pyrometamorphic Hatrurim Complex, Part II: Zadovite, $BaCa_6[(SiO_4)(PO_4)](PO_4)_2F$, and aradite, $BaCa_6[(SiO_4)(VO_4)](VO_4)_2F$, from paralavas of the Hatrurim Basin, Negev Desert, Israel. *Mineralogical Magazine*, **79**, 1073–1087.

Galuskin E.V., Galuskina I.O., Gfeller F., Krüger B., Kusz J., Vapnik J., Dulski M. and Piotr Dżierzanowski P. (2016) Silicocarnotite, $Ca_5[(SiO_4)(PO_4)](PO_4)$, a new 'old' mineral from the Negev Desert, Israel, and the ternesite–silicocarnotite solid solution: indicators of high-temperature alteration of pyrometamorphic rocks of the Hatrurim Complex, Southern Levant. *European Journal of Mineralogy*, **28**, 105–123.

Galuskin E.V., Gfeller F., Galuskina I.O., Armbruster T., Krzątała A., Vapnik Ye., Kusz J., Dulski M., Gardocki M., Gurbanov A.G. and Dzierżanowski P. (2017) New minerals with a modular structure derived from hatrurite from the pyrometamorphic rocks. Part III. Gazeevite, $BaCa_6(SiO_4)_2(SO_4)_2O$, from Israel and the Palestine Autonomy, South Levant, and from South Ossetia, Greater Caucasus. *Mineralogical Magazine*, **81**, 499–513.

Galuskin E.V., Krüger B., Galuskina I.O., Krüger H., Vapnik Y., Pauluhn A. and Olieric V. (2018*a*) Stracherite, $BaCa_6(SiO_4)_2[(PO_4)(CO_3)]F$, the first CO_3-bearing intercalated hexagonal antiperovskite from Negev Desert, Israel. *American Mineralogist*, **103**(10), 1699–1706.

Galuskin E.V., Krüger B., Galuskina I.O., Krüger H., Vapnik Y., Wojdyla J.A. and Murashko M. (2018*b*) New mineral with modular structure derived from hatrurite from the pyrometamorphic rocks of the Hatrurim complex: ariegilatite, $BaCa_{12}(SiO_4)_4(PO_4)_2F_2O$, from Negev desert, Israel. *Minerals*, **8**(3), article number 109. https://doi.org/10.3390/min8030109

Gfeller F., Galuskin E.V., Galuskina I.O., Armbruster T., Vapnik Ye., Włodyka R. and Dzierżanowski P. (2013) Natural $BaCa_6[(SiO_4)(PO_4)](PO_4)_2F$ with a new modular structure type. Goldschmidt 2013 Conference Abstracts. *Mineralogical Magazine*, **77**, 1160; https://doi.org/10.1180/minmag.2013.077.5.7

Gross S. (1977) The mineralogy of the Hatrurim Formation, Israel. *Geological Survey of Israel Bulletin*, **70**, 1–80.

Krivovichev S.V. (2008) Minerals with antiperovskite structure: a review. *Zeitschrift für Kristallographie*, **223**, 109–113.

Krüger H. (2010) $Ca_{5.45}Li_{3.55}[SiO_4]_3O_{0.45}F_{1.55}$ and $Ca_7K[SiO_4]_3F_3$: single-crystal synthesis and structures of two trigonal oxyfluorides. *Zeitschrift für Kristallographie – Crystalline Materials*, **225**, https://doi.org/10.1524/zkri.2010.1268

Mandarino J.A. (1981) The Gladstone-Dale relationship: Part lV. The compatibility concept and its application. *The Canadian Mineralogist*, **19**, 441–450.

Nishi F. and Takéuchi Y. (1984) The rhombohedral structure of tricalcium silicate at 1200°C. *Zeitschrift für Kristallographie*, **168**, 197–212.

Novikov I., Vapnik Ye. and Safonova I. (2013) Mud volcano origin of the Mottled Zone, South Levant. *Geoscience Frontiers*, **4**, 597–619.

Sheldrick G.M. (1996) *SADABS*. University of Göttingen, Germany.

Sheldrick G.M. (2008) A short history of SHELX. *Acta Crystallographica A*, **64**, 112–122.

Środek D., Dulski M. and Galuskina I. (2018) Raman imaging as a new approach to dentification of the mayenite group minerals. *Scientific Reports*, **8**(1), article number 13593. https://doi.org/10.1038/s41598-018-31809-4

Sokolova E.V., Yamnova N.A., Egorov-Tismenko Y.K. and Khomyakov A.P. (1984) The crystal structure of a new sodium-calcium-barium phosphate of Na, Ca and Ba $(Na_5Ca)Ca_6Ba(PO_4)_6F_3$. *Doklady Akademii Nauk SSSR*, **274**, 78–83.

Vapnik Y., Sharygin V.V., Sokol E.V. and Shagam R. (2007) Paralavas in a combustion metamorphic complex: Hatrurim Basin, Israel. *Reviews in Engineering Geology*, **18**, 1–21.